A library of atomically thin metal chalcogenides

Zhou, Jiadong; Lin, Junhao; Huang, Xiangwei; Zhou, Yao; Chen, Yu; Xia, Juan; Wang, Hong; Xie, Yu; Yu, Huimei; Lei, Jincheng; Wu, Di; Liu, Fucai; Fu, Qundong; Zeng, Qingsheng; Hsu, Chuang-Han; Yang, Changli; Lu, Li; Yu, Ting; Shen, Zexiang; ...Liu, Zheng

2018

Zhou, J., Lin, J., Huang, X., Zhou, Y., Chen, Y., Xia, J., . . . Liu, Z. (2018). A library of atomically thin metal chalcogenides. Nature, 556(7701), 355-359. doi:10.1038/s41586-018-0008-3

https://hdl.handle.net/10356/84198

https://doi.org/10.1038/s41586-018-0008-3

A Library of Atomically-thin Metal Chalcogenides

Jiadong Zhou[1†], Junhao Lin[2†*], Xiangwei Huang[3], Yao Zhou[4], Yu Chen[5], Juan Xia[5], Hong Wang[1], Yu Xie[6], Huimei Yu[7], Jincheng Lei[6], Di Wu[8,9], Fucai Liu[1], Qundong Fu[1], Qingsheng Zeng[1], Chuang-Han Hsu[8,9], Changli Yang[3,10], Li Lu[3,10], Ting Yu[5], Zexiang Shen[5], Hsin Lin[8,9], Boris I. Yakobson[6], Qian Liu[4], Kazu Suenaga[2], Guangtong Liu[3]* and Zheng Liu[1,11,12]*

[1]Center for Programmable Materials, School of Materials Science and Engineering, Nanyang Technological University, Singapore 639798, Singapore.

[2]National Institute of Advanced Industrial Science and Technology (AIST), Tsukuba 305-8565, Japan

[3]Beijing National Laboratory for Condensed Matter Physics, Institute of Physics, Chinese Academy of Sciences, Beijing 100190, China

[4]The State Key Laboratory of High Performance Ceramics and Superfine Microstructure, Shanghai Institute of Ceramics, Chinese Academy of Sciences, Shanghai 200050, China

[5]Division of Physics and Applied Physics, School of Physical and Mathematical Sciences, Nanyang Technological University, Singapore 637371, Singapore

[6]Department of Materials Science & Nano Engineering, Rice University, Houston, TX, USA

[7]School of Materials Science and Engineering, East China University of Science and Technology, No. 130 Meilong Road, Shanghai, China 200237

[8]Centre for Advanced 2D Materials and Graphene Research Centre, National University of Singapore, Singapore 117546

[9]Department of Physics, National University of Singapore, Singapore 117542

[10]Collaborative Innovation Center of Quantum Matter, Beijing 100871, China

[11]Centre for Micro-/Nano-electronics (NOVITAS), School of Electrical & Electronic Engineering, Nanyang Technological University, 50 Nanyang Avenue, Singapore 639798, Singapore

[12]CINTRA CNRS/NTU/THALES, UMI 3288, Research Techno Plaza, 50 Nanyang Drive, Border X Block, Level 6, Singapore 637553, Singapore

[†]These authors contributed equally to this work.

Two-dimension (2D) transition-metal chalcogenides (TMCs), due to their versatile nature, present a diversified inventory for exploring their novel physical phenomena and potential applications including quantum-spin Hall effect (QSH)[1,2], valley polarization[3,4], 2D superconductivity[5], functional devices[6-10], etc. However, only a few of them, such as Mo- and

W-based TMCs, have been synthesized via sulfurization[11-15], selenization[16,17] and tellurization[18] of metals and metal compounds. It is difficult to produce many other TMCs because of the high melting points of their metal and metal oxides precursors. Molten salt-assisted method has been widely used to produce ceramic powders at relatively low temperature[19]. Recently, it was employed to facilitate the growth of monolayer WS_2 and WSe_2 by Goki Eda etc[20]. Here, we demonstrate a universal molten salt-assisted chemical vapor deposition method for synthesizing a 2D TMCs library of 47 compounds, including 32 binary (Ti-, Zr-, Hf-, V-, Nb-, Ta-, Mo-, W-, Re-, Pt-, Pd- and Fe-based), 13 alloys (including 11 ternary, 1 quaternary and 1 quinary), and 2 heterostructured compounds. We elaborate the general growing mechanism of this method and demonstrate that the salt decreases the melting point of reactants and facilitates the formation of intermediate products, guaranteeing the successful reactions. This work paves the way for the multidisciplinary exploration of 2D TMCs across materials science, physics and various applications.

Figure 1 proposes a general picture for the synthesis of 2D TMCs by chemical vapor deposition method (CVD), based on the competition between mass flux of metal precursors and reaction rate of the domains. The mass flux determines the amount of metal precursors involved into the reaction for the formation of nucleus and the growth of domains, while the growth rate dominates the grain size of the as-grown films. At high mass flux, low growth rate results in monolayer polycrystalline film (Route I) with small grain, and high growth rate tends to form continuous monolayer films with large grain (up to millimeter size, Route II)[21]. On the other hand, at low mass flux, low growth rate leads to form small flakes. Tiny nucleus are often observed at the center of the flakes[22], suggesting that the extra adatoms or atom clusters will consistently attach to an existing nucleus or the edge during the growth (Route III). While high reaction rate prefers to produce individual

large single crystalline 2D monolayer (Route IV)[23]. Unfortunately, for many TMCs, such as Nb, Pt and Ti based ones, it is very difficult to produce them because their metal or metal oxides precursors have high melting points and low vapor pressure, which lead to very low mass flux and limit the occurrence of the reaction. Molten salt can increase their mass flux by reducing the melting points of the metal precursors and forming oxychlorides via reacting with some metal oxides, and finally facilitate the reactions. Based on this, we demonstrate a 2D TMCs library of 2D metal chalcogenides as shown in Fig. 2.

Figure 2a shows a schematic of the periodic table highlighting the chemical combination of all produced 2D TMC atomic layers, formed between 12 transition-metal (purple) and 3 chalcogens (yellow). Synthetic recipes and reaction conditions are illustrated in the Method sections, and are summarized in Fig. S1 and Table S1. Figure 2b shows optical images of 47 2D TMC compounds with morphologies of triangles, hexagons, ribbons and films, including 32 binary crystal from IVB (Ti, Zr and Hf) to VIII (Pd and Pt) group, 13 alloyed TMCs (containing ternary, quaternary even quinary compounds) which are important for universal band gap engineering and heterogeneous catalysis[24-27], and 2 heterostructure TMCs (vertically stacked $MoS_2/NbSe_2$ and in-plane 1T′ $MoTe_2$ - 2H $MoTe_2$). Star makers in the panels highlight the new 2D TMCs that have not yet been synthesized before. The detailed characterizations of all 2D TMCs and heterostructures are presented in Fig. S2-S11.

The atomic structures and chemical compositions of the as-synthesized 2D crystals and compounds are further revealed by atom-resolved STEM imaging, energy-dispersive X-ray spectroscopy (EDS) and electron energy loss spectroscopy (EELS). The atomic structures of most 2D crystals can be classified into four types: (1) trigonal prismatic 1H phase; (2) the undistorted 1T phase with the metal atom located at the center of an octahedral unit; (3) the one-dimensional

distorted 1T phase (called 1T′ phase), where pairs of metal atoms move closer to each other perpendicularly, resulting in quasi-one-dimensional chain-like structure consisting of distorted octahedral units; (4) and the two-dimensional distorted 1T phase (called 1T″ phase), where four nearby metal atoms move closer to each other as a new unit cell, forming repeatable diamond-like patterns. The structural phase of each synthesized material can be determined by the Z-contrast STEM image. Figure 3a-3d show the representative materials for each phase; these are monolayer MoS_2, $PtSe_2$, WTe_2 and $ReSe_2$ for the 1H, 1T, 1T′ and 1T″ phases with the corresponding atomic structural models, respectively. The patterns obtained by fast Fourier transform (FFT) further indicate that the 1H and 1T phases maintain a hexagonal unit cell, whereas the 1T′ phase forms a rectangular unit cell due to one-dimensional metal-pair distortion and 1T″ phase changes to a much larger hexagonal cell due to the aggregation of four metal atoms as a new unit. A summary of different phases for each as-synthesized 2D material that have been examined is shown in Fig. S12. Details of the atomic structure, EDS and EELS characterizations for each 2D crystal are shown in the Supplementary Information Fig. S13 - S27.

STEM image of a quinary $V_xW_yMo_{1-x-y}S_{2z}Se_{2(1-z)}$ monolayer alloy is shown in Fig. 3e, where the chemical composition is verified by the EDS spectrum (Fig. 3f). Corresponding optical image and Raman spectrum are shown in Fig. S9. Different chemical species give rise to the distinct atomic contrast in the image. Combined with the intensity histogram analysis of the cation and anion sites (Fig. S28), each atomic column can be directly assigned with their chemical identities by their image contrast, as shown by the representative line intensity profile in Fig. 3g. The atom-by-atom mapping further confirms the successful synthesis of a quinary alloyed monolayer. We also observe the superconductivity in monolayer $NbSe_2$ and $MoTe_2$ (Fig. S29 to Fig. S31),[28,29] the realization of superconductivity in non-UHV-grown monolayer materials. Combining with the

high mobility of monolayer MoS_2 and ReS_2 (Fig. S32 and Fig. S33), these results indicate the high quality of the as-prepared 2D TMCs. It is worth noting that the majorities of the as-synthesized materials show well control in thickness and nice quality, while a few types of 2D TMCs such as $ZrTe_2$, $TiTe_2$, $HfTe_2$ and Pd-based ones need to be further improved.

The growing mechanism of the salt-assisted CVD method is discussed in Fig. 4 and detailed in supplementary information (Fig. S34 to Fig. S53). Figure 4a illustrates that salt can reduce the melting points of metal precursors, and thus make the reaction possible (also see Fig. S35) to grow 2D TMCs. As an example, comparison of observed Nb-nucleus with and without adding salt is shown in Fig. 4a, indicating a high mass flux of metal precursors promoted by the salt. In addition to decreases of the melting point, Fig. 4b shows that some metal oxides can react with salt to form metal oxychlorides, which evaporate at an appropriate temperature and facilitate the growth of the 2D TMCs. We obtained the melting points of the precursors for all binary 2D systems by TG-DSC measurements. They all located at the temperature window from 600 to 850 °C as shown in Fig. 4c, which perfectly fits the growing temperature of the corresponding materials. This is further supported by the TG *vs* time curves in Fig. 4d. During the growth, coarsening forms a stable nucleus (Fig. S38), then adatoms and atom clusters of chalcogen and metal attach to the edges of as-growing 2D monolayers for a fast growth due to their high mobility (Fig. S47 and Fig. S48). This growth process is supported by our experimental evidence (Fig. S49-S51), and also previous reports on MoS_2[30]. This helps to produce millimeter-sized single-crystal 2D TMCs, like W, Nb and Mo-based ones (Fig 4b). Notably, the growth time in our experiment is as short as 3 min and the growth rate is up to 8 μm/s (Fig. S39-S40), due to the high chemical activities of oxychloride during the reaction. In order to confirm the existence of metal oxychloride, the intermediate products are collected and analyzed by XPS during the synthesis of monolayer NbX_2, MoX_2, and

WX_2(X: S, Se, Te). The signals from M-Cl and M-O (M: W, Nb, Mo) bonds in Nb *3d*, Mo *3d* and W *4f* (Fig. 4e, 4f and 4g) confirm the existence of the oxychloride compounds of NbO_xCl_y, MoO_xCl_y, and WO_xCl_y [31-33](see also Fig. S42- S43). Moreover, the formation of metal oxychloride is also corroborated by *ab initio* molecular dynamics simulations (Fig. S26 and Fig. S27). The density functional theory calculations show that it is energetically more favorable to sulfurize metal oxychlorides than metal oxides.

In conclusion, we have demonstrated a universal salt-assisted CVD method for producing 2D TMC library consisting of 47 compounds and heterostructures. Our work provides a swift way to produce good quality 2D TMCs and also comprehensive understanding for the growing mechanism, which will offer new possibilities to explore their extraordinary physical phenomena and novel nanodevices applications.

Reference

1 Zhang, Y. B., Tan, Y. W., Stormer, H. L. & Kim, P. Experimental observation of the quantum Hall effect and Berry's phase in graphene. *Nature* **438**, 201-204, (2005).

2 Qian, X. F., Liu, J. W., Fu, L. & Li, J. Quantum spin Hall effect in two-dimensional transition metal dichalcogenides. *Science* **346**, 1344-1347, (2014).

3 Xiao, D., Liu, G. B., Feng, W. X., Xu, X. D. & Yao, W. Coupled Spin and Valley Physics in Monolayers of MoS_2 and Other Group-VI Dichalcogenides. *Phys Rev Lett* **108**, 196802 (2012).

4 Zeng, H. L., Dai, J. F., Yao, W., Xiao, D. & Cui, X. D. Valley polarization in MoS_2 monolayers by optical pumping. *Nat Nanotechnol* **7**, 490-493, (2012).

5 Saito, Y., Nojima, T. & Iwasa, Y. Highly crystalline 2D superconductors. *Nat Rev Mater* **2**, (2017).

6 Novoselov, K. S. *et al.* Electric field effect in atomically thin carbon films. *Science* **306**, 666-669, (2004).

7 Radisavljevic, B. & Kis, A. Mobility engineering and a metal-insulator transition in monolayer MoS_2. *Nat Mater* **12**, 815-820, (2013).

8 Wang, Q. H., Kalantar-Zadeh, K., Kis, A., Coleman, J. N. & Strano, M. S. Electronics and optoelectronics of two-dimensional transition metal dichalcogenides. *Nat Nanotechnol* **7**, 699-712, (2012).

9 Roy, K. *et al.* Graphene-MoS2 hybrid structures for multifunctional photoresponsive memory devices. *Nat Nanotechnol* **8**, 826-830, (2013).

10 Lopez-Sanchez, O., Lembke, D., Kayci, M., Radenovic, A. & Kis, A. Ultrasensitive photodetectors based on monolayer MoS_2. *Nat Nanotechnol* **8**, 497-501, (2013).

11 Zhan, Y. J., Liu, Z., Najmaei, S., Ajayan, P. M. & Lou, J. Large-Area Vapor-Phase Growth and Characterization of MoS_2 Atomic Layers on a SiO2 Substrate. *Small* **8**, 966-971, (2012).

12 van der Zande, A. M. *et al.* Grains and grain boundaries in highly crystalline monolayer molybdenum disulphide. *Nat Mater* **12**, 554-561, (2013).
13 Lee, Y. H. *et al.* Synthesis of Large-Area MoS_2 Atomic Layers with Chemical Vapor Deposition. *Adv Mater* **24**, 2320-2325, (2012).
14 Lin, Y. C. *et al.* Wafer-scale MoS_2 thin layers prepared by MoO_3 sulfurization. *Nanoscale* **4**, 6637-6641, (2012).
15 Elias, A. L. *et al.* Controlled Synthesis and Transfer of Large-Area WS_2 Sheets: From Single Layer to Few Layers. *Acs Nano* **7**, 5235-5242, (2013).
16 Lu, X. *et al.* Large-Area Synthesis of Monolayer and Few-Layer $MoSe_2$ Films on SiO_2 Substrates. *Nano Lett* **14**, 2419-2425, (2014).
17 Huang, J. K. *et al.* Large-Area Synthesis of Highly Crystalline WSe_2 Mono layers and Device Applications. *Acs Nano* **8**, 923-930, (2014).
18 Park, J. C. *et al.* Phase-Engineered Synthesis of Centimeter-Scale 1T'- and 2H-Molybdenum Ditelluride Thin Films. *Acs Nano* **9**, 6548-6554, (2015).
19 Kimura, T. Molten Salt Synthesis of Ceramic Powders. *ADVANCES IN CERAMICS*-SYNTHESIS AND CHARACTERIZATION PROCESSING AND SPECIFIC APPLICATIONS. (ed. Sikalidis, C) Ch. **2** (InTech, 2011).
20 Li, S. S. *et al.* Halide-assisted atmospheric pressure growth of large WSe_2 and WS_2 monolayer crystals. *Applied Materials Today* **1**, 60-66, (2015).
21 Dumcenco, D. *et al.* Large-Area Epitaxial Mono layer MoS_2. *Acs Nano* **9**, 4611-4620, (2015).
22 Li, B. *et al.* Solid-Vapor Reaction Growth of Transition-Metal Dichalcogenide Monolayers. *Angew Chem Int Edit* **55**, 10656-10661, (2016).
23 Gong, Y. J. *et al.* Synthesis of Millimeter-Scale Transition Metal Dichalcogenides Single Crystals. *Adv Funct Mater* **26**, 2009-2015, (2016).
24 Chen, Y. F. *et al.* Tunable Band Gap Photoluminescence from Atomically Thin Transition-Metal Dichalcogenide Alloys. *Acs Nano* **7**, 4610-4616, (2013).
25 Gong, Y. J. *et al.* Band Gap Engineering and Layer-by-Layer Mapping of Selenium-Doped Molybdenum Disulfide. *Nano Lett* **14**, 442-449, (2014).
26 Lin, Z. *et al.* Facile synthesis of MoS_2 and $Mo_XW_{1-x}S_2$ triangular monolayers. *Apl Mater* **2**, 092514 (2014).
27 Azizi, A. *et al.* Spontaneous Formation of Atomically Thin Stripes in Transition Metal Dichalcogenide Monolayers. *Nano Lett* **16**, 6982-6987, (2016).
28 Xi, X. X. *et al.* Ising pairing in superconducting $NbSe_2$ atomic layers. *Nat Phys* **12**, 139-143, (2016).
29 Xi, X. X. *et al.* Strongly enhanced charge-density-wave order in monolayer $NbSe_2$. *Nat Nanotechnol* **10**, 765-769, (2015).
30 Fei, L. *et al.* Direct TEM observations of growth mechanisms of two-dimensional MoS_2 flakes. *Nat Commun* **7**, 12206, (2016).
31 CHEN*, H.-M. W. a. S.-A. Facile synthesis of MoS_2 and $Mo_XW_{1-x}S_2$ triangular monolayers.
32 Alov, N. V. XPS study of MoO_3 and WO_3 oxide surface modification by low-energy Ar+ ion bombardment. *Physica Status Solidi C: Current Topics in Solid State Physics, Vol 12, No 3* **12**, 263-266, (2015).
33 Mcguire, G. E., Schweitz.Gk & Carlson, T. A. Study of Core Electron Binding-Energies in Some Group Iiia, Vb, and Vib Compounds. *Inorg Chem* **12**, 2450-2453, (1973).

Supplementary Information is available in the online version of the paper

Acknowledgements This work is supported by the Singapore National Research Foundation under NRF RF Award No. NRF-RF2013-08, Tier 2 MOE2016-T2-2-153, MOE2016-T2-1-131, MOE2015-T2-2-007, Tier 1 RG164/15, T1-001-075, CoE Industry Collaboration Grant

WINTECH-NTU and A*Star QTE programme. J.L. and K.S. acknowledge JST-ACCEL and JSPS KAKENHI (JP16H06333 and P16382) for financial support. The work in SICCAS was supported by the National Key Research and Development Program of China ((2016YFB0700204)) and the Nation Natural Science Foundation of China (51502327). The work at IOP was supported by the Ministry of Science and Technology of China (Nos.2014CB920904, 2015CB921101, and 2013CB921702), the National Natural Science Foundation of China (Nos. 11174340, 912212012, 11527806 and 91421303) and the Chinese Academy of Sciences (No. XDB07010100). H.L. acknowledges the Singapore National Research Foundation for the support under NRF Award No. NRF-NRFF2013-03. T.Y. acknowledges MOE tier 1: RG100/15.

Author contributions J.Z., Z.L. designed the experiments. J.Z worked on the growth of the materials without ($TiSe_2$ $NbSe_2$ and $TaSe_2$, H.W worked). Y.C, J.X., J.Z. T.Y and Z. S carried out Raman characterizations. J.L. and K.S. performed the STEM characterizations of all samples and analysis. J.Z performed the AFM characterization of the samples. Y.Z., H.Y and Q.L performed the TG-DSC and XPS test. Y.X, J.C.L. and B.I.Y. worked on the molecular dynamics simulations. T.R.C., C.-H.C, D.W., H.T.J, and H.L. performed electronic structure calculations. X.H, Q.Z., F.L., and Q.F. fabricated the devices. X.H., G.L., C.Y. and L.L. measured the superconductivity in $MoTe_2$ and $NbSe_2$. J.Z., J.L. and Z.L. wrote the paper. All authors discussed and commented on the manuscript.

Author Information Reprints and permissions information is available at www.nature.com/reprints. The authors declare no competing financial interests. Readers are welcome to comment on the online version of the paper. Correspondence and requests for materials should be addressed to J.L. (email: lin.junhao@aist.go.jp) or G.L. (email: gtliu@iphy.ac.cn) or Z.L. (email: z.liu@ntu.edu.sg).

Figure Legends:

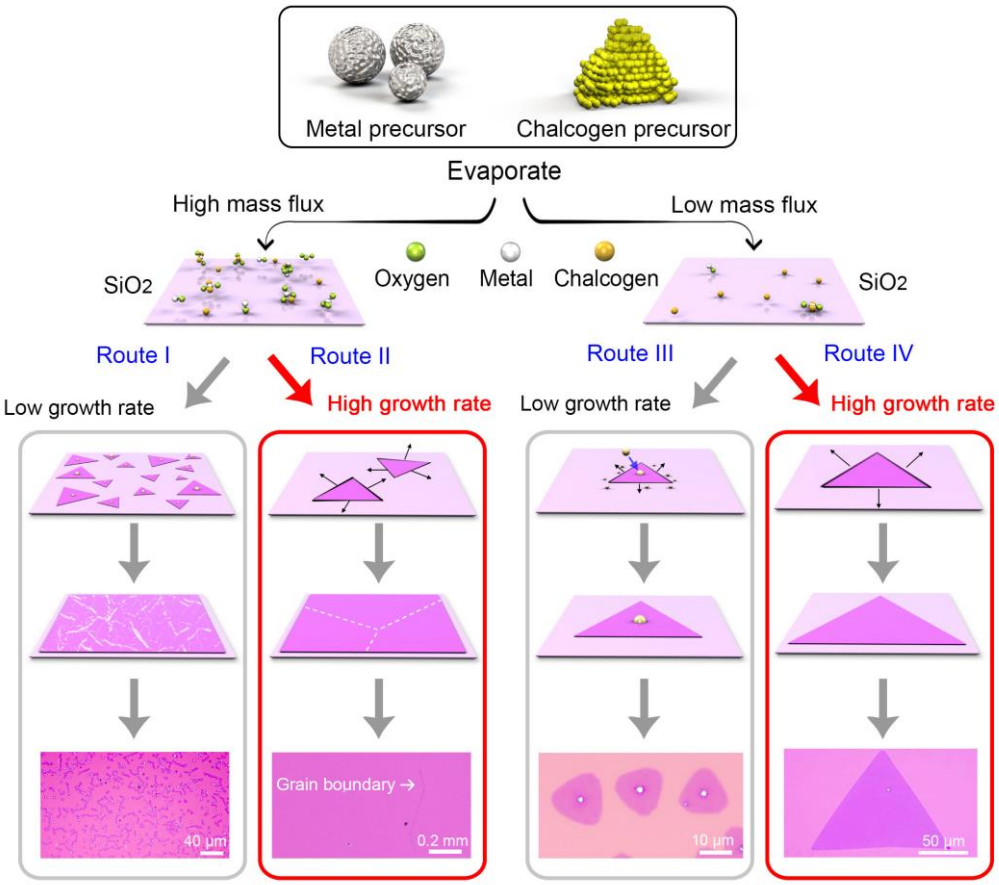

Figure 1 | Flow chart of the general growing process for the produce of TMCs by CVD method. The growth of 2D TMCs can be classified into four routes based on different mass flux of metal precursor and growth rate. High mass flux of metal precursor offers the opportunity to synthesize large-scale continuous monolayer polycrystalline film with small (route I) or large domains (route II) depending on the growth rate. On the other hand, low mass flux of metal precursor results in discrete single crystalline monolayers with different sizes. Low growth rate leads to small size with atom clusters decorated in the center and edge (route III), while high growth rate gives rise to monocrystal with large area (route IV).

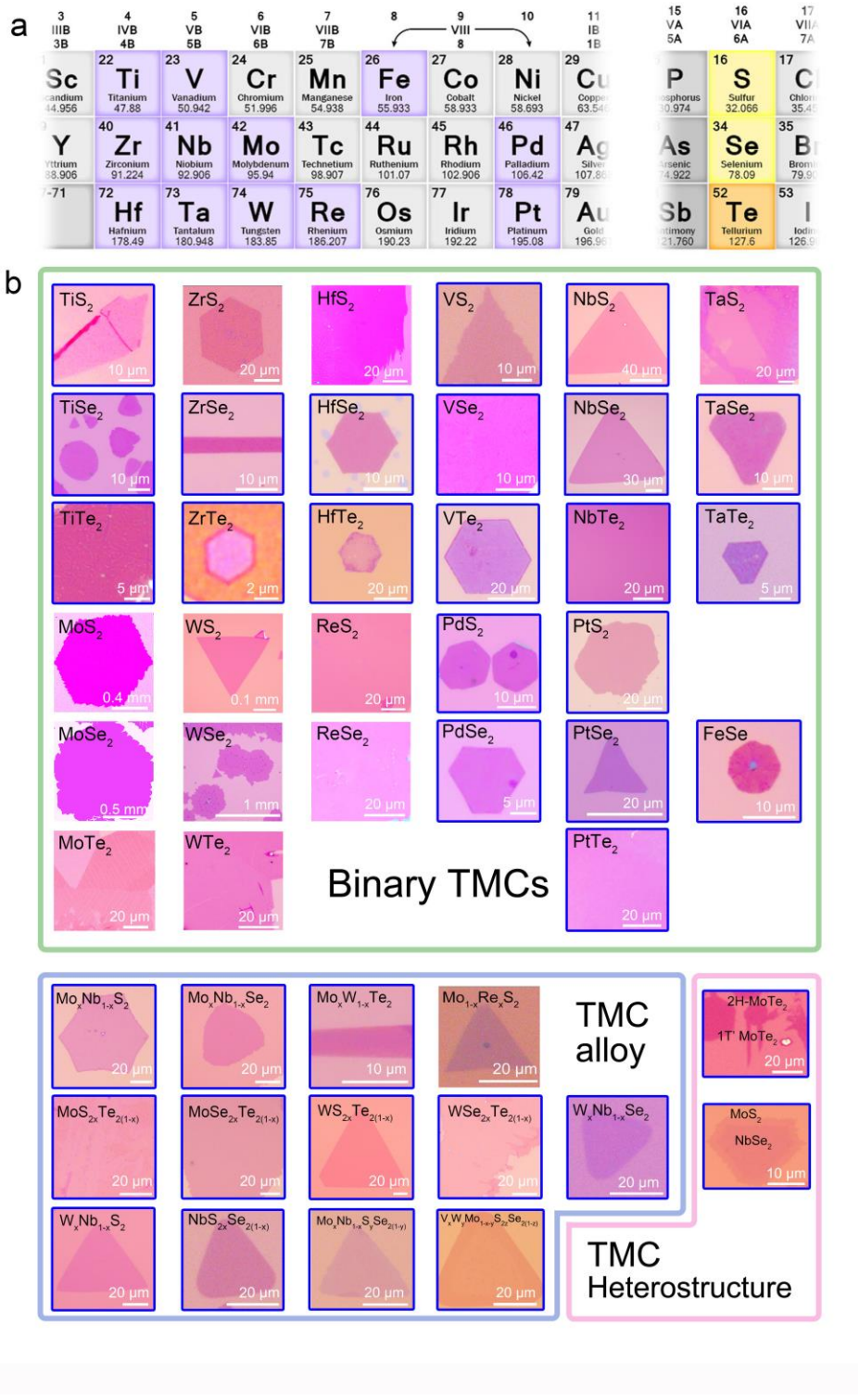

Figure 2 | Optical images of 47 different atom-thin TMCs and heterostructures. a, Overview of metals (highlighted in purple) and chalcogens (highlighted in yellow) that can form layered

sulfides, selenides and tellurides. **b**, Optical images of 47 TMCs synthesized using our method: (1) binary 2D crystals containing Mo (MoS_2, $MoSe_2$, $MoTe_2$), W (WS_2, WSe_2, WTe_2), Re (ReS_2, $ReSe_2$), Ti (TiS_2, $TiSe_2$, $TiTe_2$), Zr (ZrS_2, $ZrSe_2$, $ZrTe_2$), Hf (HfS_2, $HfSe_2$, $HfTe_2$), V (VS_2, VSe_2, VTe_2), Nb (NbS_2, $NbSe_2$, $NbTe_2$), Ta (TaS_2, $TaSe_2$, $TaTe_2$), Pt (PtS_2, $PtSe_2$, $PtTe_2$), Pd (PdS_2, $PdSe_2$), FeSe; (2) ternary alloys containing MoS_xTe_{2-x}, $MoSe_xTe_{2-x}$, WS_xTe_{2-x}, WSe_xTe_{2-x}, NbS_xSe_{2-x}, $Mo_xNb_{1-x}S_2$, $Mo_xNb_{1-x}Se_2$, $Mo_{1-x}Re_xS_2$, $W_xNb_{1-x}S_2$, $W_xNb_{1-x}Se_2$, $Mo_xW_{1-x}Te_2$; (3) quaternary alloy $Mo_xNb_{1-x}S_{2y}Se_{2(1-y)}$; (4) quinary alloy $V_xW_yMo_{1-x-y}S_{2z}Se_{2(1-z)}$; (5) 1T′ $MoTe_2$ – 2H $MoTe_2$ in-plane and MoS_2-$NbSe_2$ vertically stacked heterostructures. New TMCs that have not been synthesized before are indicated by a star maker. Detailed characterizations on the as-grown 2D materials are shown in the Supplementary Information.

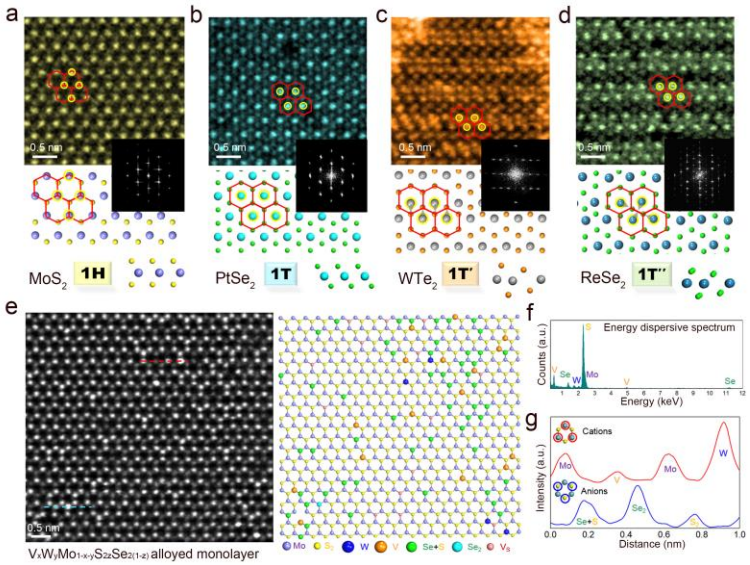

Figure 3 | Atomic-resolution STEM images of representative monolayer materials in different phases. a-d, MoS_2 in the 1H phase, $PtSe_2$ in the 1T phase, WTe_2 in the 1T′ phase and $ReSe_2$ in the 1T″ phase, with the corresponding FFT patterns and atomic structural models, respectively. e, STEM image of quinary monolayer alloy: $V_xW_yMo_{1-x-y}S_{2z}Se_{2(1-z)}$. f, EDS spectra of the alloyed monolayer, confirming its chemical composition. g, Line intensity profiles along the

highlighted red (cation) and blue (anion) dashed lines in (e), indicating the different intensity of each chemical species.

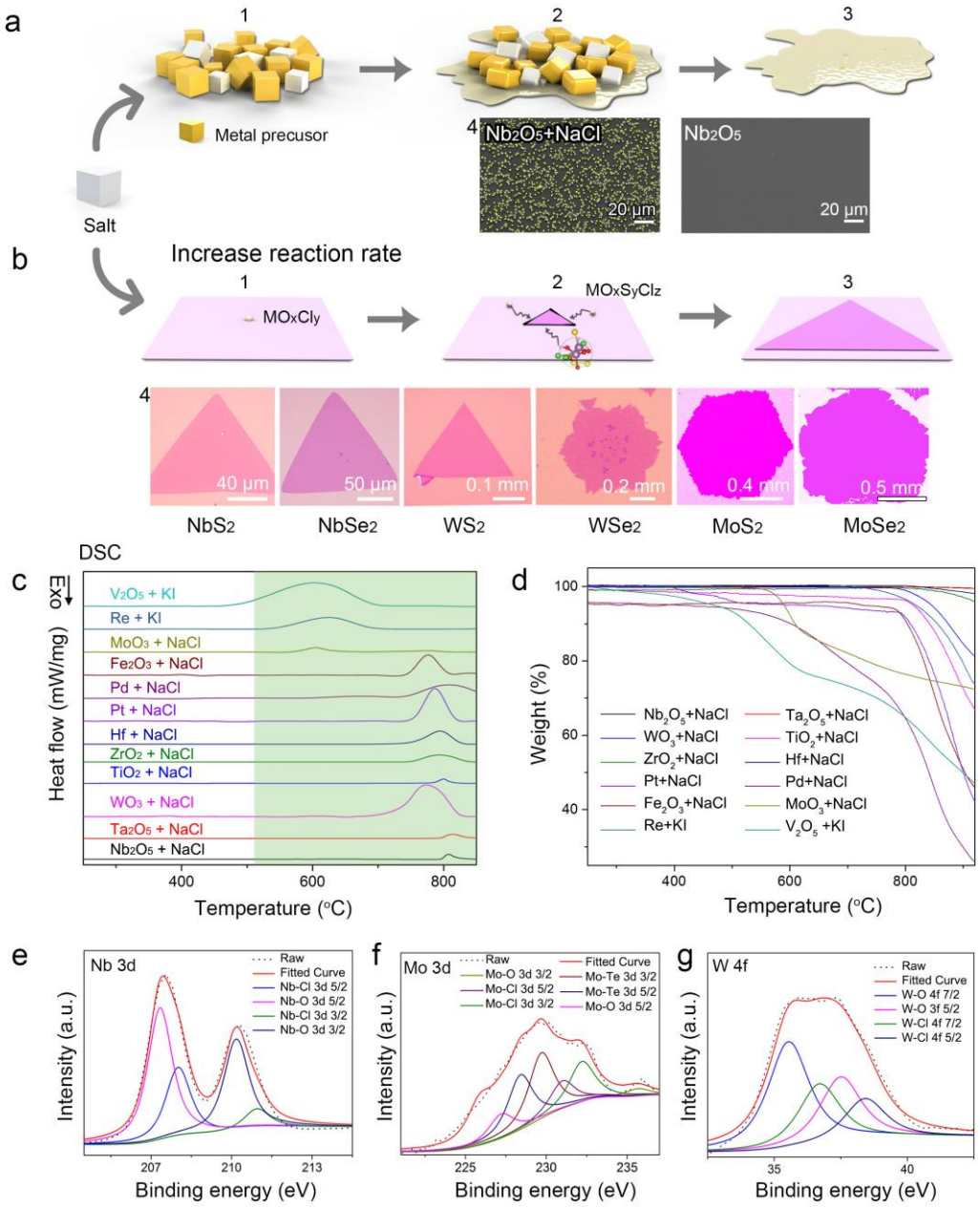

Figure 4 | Reaction mechanism. a-b, Schematic of the reactions. Metal oxychlorides are formed which promote the reactions. Chalcogens are not shown here. 1-3, the proposed process of the decreased melting point of precursors assisted by salt. 4, SEM images of Nb-nucleus with and

without adding salt. **b**, 1-3, the growth process of 2D atomic layer with the intermediate products; 4, different single crystalline monolayers with large size and a growth time less than 3 min. **c** and **d**, TG-DSC curve of mixed salt with the metal sources. The measurement of melting points of the systems after mixing with salt are all within the highlighted windows from 600 to 850 °C. **e** – **g**, XPS spectra showing the existence of the Cl bonds to other elements, resulting from the intermediate products during the synthesis of Nb- , Mo-and W-based 2D crystals.

METHODS

Synthesis Recipe -The 2D compounds and heterostructures were synthesized in a quartz tube with 1 inch in diameter. The length of the furnace is about 36 cm. The system of the reaction is shown in Fig. S32. Mixed gas of H_2/Ar was used as the carrier gas. Specifically, the alumina boat with the volume about 8cm X 1.1 cm X 1.2 cm containing precursor powder was put in the center of the tube. The precursor powder and the salt were mixed together first. The Si substrate with 285 nm SiO_2 top layer was placed on the alumina boat with surface down, the distance between the sources and substrate ranges from 0.2 cm to 1.2 cm. Another alumina boat containing S or Se or Te powder was put on the upstream of tube furnace at 200 ^oC, 300 ^oC, and 450 ^oC, respectively. The distance between the S or Se or Te boat and the precursor's boat is about 18 cm, 16 cm, and 15 cm, respectively. The heating rate of all reactions is 50 ^oC/min. All the reactions were carried out at atmospheric pressure. The temperature was cooled down to room temperature naturally. All reaction materials were bought from Alfa Aesar with purity more than 99%.

MoS_2: Mixed powder of NaCl (0.5 mg) and MoO_3 (3 mg) in alumina boat was placed in the center of the tube. The furnace was heated to the growing temperature (600 to 800 ^oC) with a ramp rate of 50 ^oC/min. The growth time is 3 to 5 min. The Ar (or Ar/H_2) with a flow rate of 80 (80/5) sccm was used as the carrier gas.

$MoSe_2$: The synthesis recipe for $MoSe_2$ is similar to that of MoS_2. The growth temperature was about 700-800 ^oC, and the Ar/H_2 with a flow rate of 80/5 sccm was used as the carrier gas.

$MoTe_2$: Mixed powder of NaCl (4 mg) and MoO_3 (14 mg) in the alumina boat was placed in the center of the tube. The furnace was heated to growth temperature (600 to 800 ^oC) with a ramp rate of 50 ^oC/min and held for 3 mins before cooling down to room temperature naturally. The mixed Ar/H_2 gas with a flow rate of 80/20 sccm was used as the carrier gas.

WS_2: Using our mehtod, large-size and monolayered WS_2 single crystal can be prepared at relatively low temperature of about 750 ^oC~850 ^oC. The alumina crucible containing 6 mg NaCl and 30 mg WO_3 was placed in the center of the tube. The furnace was heated with a ramp rate of 50 ^oC/min to the growth temperature (750 to 850 ^oC) and held for 3 mins. The Ar/H_2 (80/10 sccm) was used as the carrier gas.

WSe_2: The growth process of WSe_2 was similar to that of WS_2. The size of the monolayered WSe_2 single crystal can reach up to 1 mm.

WTe_2: Mixed powder of NaCl and WO_3 with weight of 15 mg and 60 mg, respectively, was placed in the center of the tube. The furnace was heated with a ramp rate of 50 ^oC/min to the growth temperature (750 to 850 ^oC) and held at this temperature for 3 mins before cooling down to room temperature naturally. The Ar/H_2 with a flow 80/20 sccm was used as the carrier gas.

TiS_2: 3 mg NaCl and 10 mg TiO_2 in the alumina boat was placed in the center of the tube. The furnace was heated with a ramp rate of 50 ^oC/min to the growth temperature (750 to 810 ^oC) and held at this temperature for 8-15 mins before cooled down to room temperature naturally. The Ar/H_2 with a flow rate of 80/20 sccm was used as the carrier gas. Based on our method, monolayer TiS_2 with a size up to 50 μm was obtained.

$TiSe_2$: The parameters for the growth of $TiSe_2$ is similar to those of TiS_2 but replacing S with Se. Ar/H_2 with a flow rate of 100/20 sccm was used as the carrier gas.

$TiTe_2$: NaCl and TiO_2 (Note that the Ti powder can be used) are mixed with a weight of 3 mg and 10 mg in the alumina boat and then placed the boat in the center of the tube. The furnace was heated with a ramp rate of 50 ^oC/min to the growth temperature (800 to 850 ^oC) and held at this temperature for 10-15 mins before cooling down to room temperature naturally. The Ar/H_2 with a flow of 110/20 sccm was used as the carrier gas.

ZrS_2: The synthesis procedures are as follows: mixed powder of NaCl and ZrO_2 (Note that the Zr powder can be used) with weight of 3 mg and 10 mg in the alumina boat was placed in the center of the tube. The furnace was heated with a ramp rate of 50 ^oC/min to the growth temperature (750 to 800 ^oC) and held at this temperature for 10-15 mins before cooled down to room temperature naturally. The Ar/H_2 with a flow rate of 100/20 sccm was used as the carrier gas.

$ZrSe_2$: Similar to the synthesis of ZrS_2 but replace S with Se powder and raise growth temperature to (750 to 830 ^oC).

$ZrTe_2$: Similar to the synthesis of ZrS_2 but replace S with Te powder and raise growth temperature to (800 to 850 ^oC).

HfS_2: The synthetic procedures are as follows: mixed powder of NaCl and Hf with weight of 3 mg and 5 mg in the alumina boat was placed in the center of quartz tube. Another alumina boat containing S powder was placed in the upstream. The furnace was heated with a ramp rate of 50 ^oC/min to the growth temperature (800 to 850 ^oC) and held at this temperature for 10-15 mins before cooled down to room temperature naturally. The Ar with a flow rate of 120 sccm was used as the carrier gas.

$HfSe_2$: Similar to the synthesis of HfS_2 but replace S with Se powder and raise growth temperature to (750 to 850 ^oC). The Ar/H_2 with a flow rate of 120/20 sccm was used as the carrier gas.

$HfTe_2$: Similar to the synthesis of HfS_2 but replace S with Te powder and raise growth temperature to (800 to 850 ^oC). The Ar/H_2 with a flow rate of 120/20 sccm was used as the carrier gas.

VS_2, VSe_2 and VTe_2: Mixed powder of KI and V_2O_5 with weight of 1 mg and 3 mg in the alumina boat was placed in the center of quartz tube. Another alumina boat containing S/Se/Te powder was placed in the upstream. The furnace was heated with a ramp rate of 50 ^oC/min to the growth

temperature (680 to 750 ^{o}C) and held at this temperature for 10-15 mins before cooled down to room temperature naturally. The Ar/H_2 with a flow rate of 80/16 sccm was used as the carrier gas.

NbS_2, $NbSe_2$ and $NbTe_2$: The mixed powder of NaCl and Nb_2O_5 with weight of 2 mg and 10 mg in the alumina boat was placed in the center of quartz tube. Another alumina boat containing S/Se/Te powder was placed in the upstream. The furnace was heated with a ramp rate of 50 ^{o}C/min to the growth temperatures (750 to 850 ^{o}C) and held at this temperature for 3-5 mins before cooled down to room temperature naturally. The Ar/H_2 with a flow rate of 80/16 sccm was used as carrier gas.

NbS_2, $NbSe_2$ and $NbTe_2$: The mixed powder of NaCl and Ta_2O_5 with weight of 5 mg and 30 mg in the alumina boat was placed in the center of the tube. Another alumina boat containing S/Se/Te powder was placed in the upstream. The furnace was heated with a ramp rate of 50 ^{o}C/min to the growth temperature (800 to 850 ^{o}C) and held at this temperature for 10-20 mins before cooled down to room temperature naturally. The Ar/H_2 with a flow rate of 100/18 sccm was used as carrier gas.

ReS_2: the mixed powder of KI and Re with weight of 1 mg and 5 mg in the alumina boat was placed in the center of the quartz tube. The furnace was heated with a ramp rate of 50 ^{o}C/min to the growth temperature (650 to 750 ^{o}C) and held for 5-10 mins before cooled down to room temperature naturally. The Ar with a flow rate of 60 sccm was used as the carrier gas.

$ReSe_2$: Despite that the synthesis of ReS_2 has been reported, the monolayer $ReSe_2$ has not been synthesized successfully. Here, the preparation method of $ReSe_2$ is similar to the synthesis of ReS_2. The Se powder was used as Se source and reaction temperature was fixed at 700~780 ^{o}C. The mixed Ar/H_2 with a flow rate of 80/10 sccm was used as carrier gas.

FeSe: Mixed powder of NaCl and Fe_2O_3 (or $FeCl_2$) with weight of 2 mg and 10 mg in the alumina boat was placed in the center of the quartz tube. Another alumina boat containing Se powder was placed in the upstream. The furnace was heated with a ramp rate of 50 ^{o}C/min to the growth temperatures (750 to 850 ^{o}C) and held at this temperature for 10-20 mins before cooling down to room temperature naturally. The Ar/H_2 with a flow rate of 100/18 sccm was used as the carrier gas.

PtS_2, $PtSe_2$, $PtTe_2$, PdS_2 and $PdSe_2$: Mixed powder of NaCl and M (Pt, Pd nanoparticles or $PtCl_2$, $PdCl_2$ powder) with the weight of 1 mg and 10 mg in the alumina boat was placed in the center of the quartz tube. Another alumina boat containing S/Se/Te powder was placed in the upstream. The furnace was heated with a ramp rate of 50 ^{o}C/min to the growth temperatures (800 to 850 ^{o}C) and held at this temperature for 10-20 mins before cooled down to room temperature naturally. The mixed Ar/H_2 with a flow of 100/20 sccm was used as the carrier gas.

$MoS_{2x}Te_{2(1-x)}$: Mixed powder of NaCl and MoO_3 with weight of 2 mg and 10 mg in the alumina boat was placed in the center of the tube. Another alumina boat containing mixed powder (S and Te) was placed in the upstream. The furnace was heated with a ramp rate of 50 ^{o}C/min to the growth temperature 700 – 800 ^{o}C and held at the temperature for 10-20 mins before cooled down to room temperature naturally. The mixed Ar/H_2 with a flow rate of 100/5 sccm was used as the carrier gas.

$MoSe_{2x}Te_{2(1-x)}$: $MoSe_{2x}Te_{2(1-x)}$ was grown using similar recipes to $MoS_{2x}Te_{2(1-x)}$ except for the mixed powder (Se and Te) as precursors.

$WS_{2x}Te_{2(1-x)}$: Mixed powder of NaCl and WO_3 with weight of 3 mg and 15 mg in the alumina boat was placed in the center of the tube. Another alumina boat containing mixed powder (S and Te) was placed in the upstream. The furnace was heated with a ramp rate of 50 ^oC/min to the growth temperature 750 – 850 ^oC and held at this temperature for 10-20 mins and then cooled down to room temperature naturally. The mixed Ar/H_2 with a flow rate of 100/5 sccm was used as the carrier gas.

$WSe_{2x}Te_{2(1-x)}$: $WSe_{2x}Te_{2(1-x)}$ was grown using similar recipes to $WS_{2x}Te_{2(1-x)}$ except for the mixed powder (Se and Te) as precursors.

$NbS_{2x}Se_{2(1-x)}$: Mixed powder of NaCl and Nb_2O_5 with weight of 2 mg and 10 mg in the alumina boat was placed in the center of the tube. The furnace was heated with a ramp rate of 50 ^oC/min to the growth temperature 760 – 840 ^oC and held at this temperature for 10-20 mins before cooled down to room temperature naturally. The mixed Ar/H_2 with a flow rate of 100/15 sccm was used as the carrier gas.

$Mo_{1-x}Nb_xSe_2$: Mixed powder of NaCl and the powder of (Nb_2O_5: MoO_3=1:1) with weight of 2 mg and 10 mg in the alumina boat was placed in the center of the tube. Another alumina boat containing Se powder was placed in the upstream. The furnace was heated with a ramp rate of 50 ^oC/min to the growth temperature 760 – 840 ^oC and held at this temperature for 10-20 mins followed by cooling down to room temperature naturally. The mixed Ar/H_2 with a flow rate of 100/15 sccm was used as the carrier gas.

$Mo_{1-x}Re_xS_2$: Mixed powder of NaCl and the powder of (Re: MoO_3=1:1) with weight of 2 mg and 10 mg in the alumina boat was placed in the center of the tube. The furnace was heated with a ramp rate of 50 ^oC/min to the growth temperature 700 – 800 ^oC and held at this temperature for 10-20 mins before cooled down to room temperature naturally. The mixed Ar/H_2 with a flow rate of 80/5 sccm was used as the carrier gas.

$W_{1-x}Nb_xS_2$: Mixed powder of NaCl and the powder of (Nb_2O_5: WO_3=1:1) with weight of 2 mg and 15 mg in the alumina boat was placed in the center of the tube. The furnace was heated with a ramp rate of 50 ^oC/min to the growth temperature 750 – 840 ^oC and held at this temperature for 10-20 mins before cooled down to room temperature naturally. The mixed Ar/H_2 with a flow rate of 100/15 sccm was used as the carrier gas.

$W_{1-x}Nb_xSe_2$: Mixed powder of NaCl and the powder of (Nb_2O_5: WO_3=1:1) with weight of 2 mg and 15 mg in the alumina boat was placed in the center of the tube. The furnace was heated with a ramp rate of 50 ^oC/min to the growth temperature 750 – 840 ^oC and held at this temperature for 10-20 mins before cooled down to room temperature naturally. The mixed Ar/H_2 with a flow rate of 100/15 sccm was used as the carrier gas.

$Mo_xNb_{1-x}S_2$: Mixed powder of NaCl and the powder of (Nb_2O_5: MoO_3=1:1) with weight of 2 mg and 10 mg in the alumina boat was placed in the center of the tube. The furnace was heated with a ramp rate of 50 ^oC/min to the growth temperature 760 – 840 ^oC and held at this temperature for 10-20 mins before cooled down to room temperature naturally. The mixed Ar/H_2 with a flow rate of 100/15 sccm was used as the carrier gas.

$Mo_xW_{1-x}Te_2$: Mixed powder of NaCl and the powder of (WO_3: MoO_3=1;1) with weight of 2 mg and 10 mg in the alumina boat was placed in the center of the tube. The furnace was heated with a ramp rate of 50 ^oC/min to the growth temperature 760 – 840 ^oC and held at this temperature for 5-

10 mins before cooled down to room temperature naturally. The mixed Ar/H_2 with a flow rate of 100/15 sccm was used as the carrier gas.

$Mo_xNb_{1-x}S_{2y}Se_{2(1-y)}$: Mixed powder of NaCl and the powder of (Nb_2O_5: MoO_3= 1:1) with weight of 2 mg and 10 mg in the alumina boat was placed in the center of the tube. Another alumina boat containing S and Se powder was placed in the upstream. The furnace was heated with a ramp rate of 50 ^oC/min to the growth temperatures 760 – 840 ^oC and held at this temperature for 10-20 mins before cooled down to room temperature naturally. The mixed Ar/H_2 with a flow rate of 100/15 sccm was used as the carrier gas.

$V_xW_yMo_{1-x-y}S_{2z}Se_{2(1-z)}$: Mixed powder of NaCl and the powder of (V_2O_5: MoO_3:WO_3=1:5:3) with weight of 2 mg and 10 mg in the alumina boat was placed in the center of the tube. Another alumina boat containing S and Se powder was placed in the upstream. The furnace was heated with a ramp rate of 50 ^oC/min to the growth temperature 760 – 840 ^oC and held at this temperature for 10-20 mins before cooled down to room temperature naturally. The mixed Ar/H_2 with a flow rate of 100/5 sccm was used as the carrier gas.

1T′ $MoTe_2$ – 2H $MoTe_2$ in-plane heterostructures: The mixed powder of NaCl (4 mg) and MoO_3 (14 mg) in the alumina boat was placed in the center of the tube. The furnace was heated to the growth temperatures 720 ^oC with a ramp rate of 50 ^oC/min and held for 3 mins, and then quickly cooled the growth temperature to 650 ^oC and held for 5 mins and then cooled down to room temperature naturally. The mixed Ar/H_2 gas with a flow rate of 80/20 sccm and 20/4 sccm was used as the carrier gas for 1T′ $MoTe_2$ and 2H $MoTe_2$ growth, respectively.

MoS_2 – $NbSe_2$ vertically stacked heterostructure: MoS_2 was synthesized firstly. The mixed powder of NaCl (0.5 mg) and MoO_3 (3 mg) in the alumina boat was placed in the center of the tube. The furnace was heated to the growing temperature (600 to 800 ^oC) with a ramp rate of 50 ^oC/min. The growth time is 3 min. The Ar (or Ar/H_2) with a flow rate of 80 (80/5) sccm was used as the carrier gas. The as-obtained MoS_2 was quickly transferred to another furnace for the heterostructure growth. For the $NbSe_2$ growth: The mixed powder of NaCl and Nb_2O_5 with weight of 2 mg and 10 mg in the alumina boat was placed in the center of the tube. Another alumina boat containing Se powder was placed in the upstream. The furnace was heated with a ramp rate of 50 ^oC/min to the growth temperature 700 ^oC and held at this temperature for 10 mins before cooled down to room temperature naturally. The Ar/H_2 with a flow rate of 60/4 sccm was used as carrier gas.

Note that the weight ratio between salt and metal precursors can be tuned. Typically, for the synthesis of alloys, we fixed the weight ratio of 1:1 for the precursors. Taking the $Mo_{1-x}Re_xS_2$ (WS_xTe_{2-x}) as examples, by tuning the ratio between Mo and Re (S and Te), we can control the value of x.

Characterizations

STEM-STEM samples were prepared with a poly (methyl methacrylate) (PMMA) assisted method or PMMA-free method with the assistance of Iso-Propyl alcohol (IPA) droplet. For some water sensitive materials, we used a non-aqueous transfer method. STEM imaging and EELS analysis were performed on a JEOL 2100F with a cold field-emission gun and an aberration corrector (the DELTA-corrector) operating at 60 kV. A Gatan GIF Quantum was used for recording the EELS spectra. The inner and outer collection angles for the STEM image (β1 and β2) were 62 and 129–

140 mrad, respectively, with a convergence semi-angle of 35 mrad. The beam current was about 15 pA for the annular dark-field (ADF) imaging and EELS chemical analyses.

TG-DSC-Thermogravimetry (TG) and Differential Scanning Calorimetry (DSC) measurements were performed using a Netzsch STA 449C thermal analyzer. Approximately 10mg of the sample was loaded into an alumina crucible and heated at 10 K min-1 from 20 to 920 °C. The 95 vol% Ar/ 5 vol% H_2 with a flow rate of 40 ml min^{-1} was used as the carrier gas.

XPS- XPS measurement was performed using a monochromated Al Kα source (hν = 1486.6 eV) and a 128 channel mode detection PHI original detector. XPS spectra were acquired at a pass energy of 140 eV and a take-off angle of 45°.

Data availability. The main data supporting the findings of this study are available within the article, and Supplementary Information. Extra data are available from the corresponding author upon request.